

Overview of image-to-image translation using deep neural networks: denoising, super-resolution, modality-conversion, and reconstruction in medical imaging

Shizuo Kaji · Satoshi Kida*

Received: date / Accepted: date

Abstract Since the advent of deep convolutional neural networks (DNNs), computer vision has seen an extremely rapid progress that has led to huge advances in medical imaging. Every year a lot of new methods are reported in conferences such as the International Conference on Medical Image Computing and Computer Assisted Intervention (MICCAI) and Machine Learning for Medical Image Reconstruction (MLMIR), or published online at the preprint server arXiv. There are a plethora of surveys on applications of neural networks in medical imaging (see [1] for a relatively recent comprehensive survey). This article does not aim to cover all the aspects of the field but focus on a particular topic of *image-to-image translation*. Although the topic may sound unfamiliar, it turns out that many seemingly irrelevant applications can be understood as instances of image-to-image translation. Such applications include (1) noise reduction, (2) super-resolution, (3) image synthesis, and (4) reconstruction. The same underlying principles and algorithms work for various tasks. Our aim is to introduce some of the key ideas on this topic from a uniform view point. We try to be less intimidating with descent level of rigour by examining core ideas using metaphors. We pay a particular attention to introducing jargons specific to image processing using DNNs. Having an intuitive grasp of the key ideas and the knowledge of technical terms would help the reader greatly to understand the existing and the future applications.

The two authors contributed equally to this work. Kaji was partially supported by JST PRESTO, Grant Number JPMJPR16E3 Japan.

S. Kaji
Institute of Mathematics for Industry, Kyushu University, Japan / JST PRESTO
E-mail: skaji@imi.kyushu-u.ac.jp

S. Kida
LPixel Inc. / The University of Tokyo hospital
E-mail: satoshikida1492@gmail.com

Most of recent applications which build on image-to-image translation base on two fundamental architectures called pix2pix and CycleGAN depending on whether the available training data are *paired* or *unpaired* (see §1.3). We provide codes ([2, 3]) which implement these two architectures with various enhancements. Our codes are available online with the very permissive MIT licence. We provide a hands-on tutorial for training a model for denoising using our codes §6. We hope this article together with the codes will provide both an overview and the details of the key algorithms and will serve as a basis for developing new applications.

Keywords deep convolutional neural networks · image-to-image translation · denoising · super-resolution · image synthesis · reconstruction

1 Image processing with deep neural networks

We begin by collecting basic notions of neural networks in general. The reader may want to skip to §1.3, where we discuss our main topic of image-to-image translation.

Conventional medical image processing algorithms rely on domain specific knowledge and assume some underlying model, and hence, each method is tailored for a specific task. On the other hand, in recent years purely data driven approaches without specific models are getting popular in medical imaging (e.g., [4, 5, 6]). In particular, *deep neural networks (DNNs)* have been proved very powerful in various image processing tasks. The most important fact for image processing is that an image is expressed by a real-valued vector. A greyscale image of dimension $w \times h$ is an element of $\mathbb{R}^{w \times h}$, where $\mathbb{R}^{w \times h}$ is the set of real-valued vectors of dimension $w \times h$. Similarly, a full colour picture of dimension $w \times h$ is an element of $\mathbb{R}^{w \times h \times 3}$ consisting of three channels corresponding to Red, Green, and Blue. This fact

allows us to apply various mathematical operations to process images. We can apply a mapping $\mathbb{R}^{w_1 \times h_1} \rightarrow \mathbb{R}^{w_2 \times h_2}$ to translate a greyscale image to another. Image filters such as Sobel filters, FFT, bilateral filters are handcrafted mappings¹, whereas DNNs are meant to find useful filters automatically from a large amount of data. DNN-based methods have achieved state-of-the-art performance in many image translation tasks, including denoising, super-resolution, image synthesis, and reconstruction.

1.1 Regression with Neural networks

In this subsection, we will explain what are neural networks and deep learning. For a good introduction to deep learning in general, look at [8]. For those who are interested in the theory of deep learning in depth, refer to [9].

Neural networks are just a particular class of multi-variate functions $f_w : \mathbb{R}^n \rightarrow \mathbb{R}^m$ with parameters (called *weights*) $w \in \mathbb{R}^l$. The parameters w are *learnable* so that they are determined by the given data through *training* in order to solve a given problem. The simplest example is the linear function $f_{(w_1, w_0)} : \mathbb{R}^1 \rightarrow \mathbb{R}^1$ defined by $f_{(w_1, w_0)}(x) = w_1 x + w_0$, whose weights are $w = (w_1, w_0) \in \mathbb{R}^2$.

Neural networks are used to approximate (*fit* or *regress*) unknown functions g from a finite number of its input-output pairs

$$\{(x_1, g(x_1)), (x_1, g(x_1)), \dots, (x_k, g(x_k))\}.$$

Here, k is the number of input-output pairs which are observed and known to us. For a new x different from x_1, \dots, x_k , we want to use $f_w(x)$ as a prediction of the unknown value $g(x)$.

To measure how well f_w approximates g , we need a *loss* function. A popular choice is the squared L^2 -distance $L(f_w, g) = \sum_{i=1}^k |f_w(x_i) - g(x_i)|^2$. A loss function is so designed that the smaller $L(f_w, g)$ is, the better f_w approximates g with respect to the loss function L . Hence, we try to find parameters w which minimise $L(f_w, g)$, or at least, which make $L(f_w, g)$ reasonably small. In case of the simplest neural network $f_{w_1, w_0}(x) = w_1 x + w_0$ with the squared L^2 -distance, this is achieved by the ordinary least squares fitting. To express more complex functions than simple linear functions, the crucial idea of neural networks is to stack (or compose) linear functions. Of course, the composition of two linear functions is again a linear function. So we need a twist, which is realised by the *activation function* (or the *non-linearity*). The simplest two-layer neural network $\mathbb{R}^1 \rightarrow \mathbb{R}^1$ is given by

$$f_w(x) = w_{2,1} \max(w_{1,1}x + w_{1,0}, 0) + w_{2,0}.$$

¹ Various image filters are implemented in the free software Fiji [7] and we can easily try them to see their characteristics.

It looks complicated but notice it is just the composition of two linear functions sandwiching the *ReLU* (Rectified Linear Unit) activation, which just outputs the input itself if it is positive and outputs zero otherwise:

$$\begin{array}{ccccc} \mathbb{R}^1 & \rightarrow & \mathbb{R}^1 & \xrightarrow{\text{ReLU}} & \mathbb{R}^1 \\ x \mapsto & y_1 = w_{1,1}x + w_{1,0} \mapsto & & & y_2 = \max(y_1, 0) \\ & & & \rightarrow & \mathbb{R}^1 \\ & & & \mapsto & y_3 = w_{2,1}y_2 + w_{2,0}. \end{array}$$

The point is that composition increases the expressive power drastically (see, for example, [10]), while keeping the building blocks rather simple (only linear functions and activation functions). Neural networks with three or more layers are referred to as *deep* neural networks (DNNs). The *universal approximation theorem* (e.g., [11]) roughly states that almost any function $g : \mathbb{R}^n \rightarrow \mathbb{R}^m$ which appear in practical applications can be approximated arbitrarily well by a deep neural network if we allow the number of weights to be arbitrarily large. Nowadays, the number of layers of a DNN is in the order of dozens and more and the parameter w lives in a high dimensional space \mathbb{R}^k with $k > 100,000,000$.

Remark 1 If three-layer networks suffice for universal approximation, why do we need dozens of layers? In practice, deeper neural networks are better at various jobs than shallower and wider neural networks with the same number of weights. However, in theory deep narrow neural networks in which width is bounded are not universal[12]. This fact poses an interesting question on how to design the structure of neural networks for a particular task.

1.2 Convolutional Neural Networks

A linear map (without a constant term) $\mathbb{R}^n \rightarrow \mathbb{R}^m$ in the general form is specified by an $m \times n$ -matrix². This means the number of weights is mn , which is huge; say, when $n = m = 256 \times 256$, the figure is over 4 million. In principle, the larger the number of weights, the more data we need to find good values of them by training. Thus, we have to keep the number relatively small based on some prior knowledge on images in general. It is reasonable to assume that two pixels far apart are independent but pixels that are next to each other are highly correlated. Also, the correlation does not depend on the absolute location of the pixel in a picture but should be similar everywhere. A mathematical tool called the *convolution* is what we need to exploit this observation. There are plenty of good expository articles on 2D *convolutional neural networks* (CNN's) (e.g., [13]), so

² Usually, a linear layer involves the constant term as well so that it has the form $x \mapsto Ax + b$ for $b \in \mathbb{R}^m$. The term b is often referred to as the *bias*.

here we present an illustrative toy case of 1D convolution. Basically, we can think of convolution as filter application with sliding window. Assume we have an input vector $x = (x_1, x_2, \dots, x_n) \in \mathbb{R}^n$. Given another vector $w = (w_1, w_2, w_3)$ called the *kernel*, we compute

$$w * x = (w_1x_1 + w_2x_2 + w_3x_3, w_1x_2 + w_2x_3 + w_3x_4, \dots, w_1x_{n-2} + w_2x_{n-1} + w_3x_n) \in \mathbb{R}^{n-2}. \quad (1.1)$$

This mapping $x \mapsto w * x$ is called the convolution with kernel w , and defines a linear mapping $\mathbb{R}^n \rightarrow \mathbb{R}^{n-2}$ with weights w . Note that the number of weights is fixed to three and independent of the dimension of the input x . The trick is that the weights are

- *sparse*; each entry of the output $w * x$ depends only three entries x_{i-1}, x_i, x_{i+1} in the input
- *shared*; the same weights w_1, w_2, w_3 are used for all entries of the output.

Next, we explain some more technical aspects of convolution. First, if we want to keep the input and the output vector sizes the same, we can use *padding* $(x_1, x_2, \dots, x_n) \mapsto (0, x_1, x_2, \dots, x_n, 0)$ so that the output (1.1) becomes

$$(w_2x_1 + w_3x_2, w_1x_1 + w_2x_2 + w_3x_3, w_1x_2 + w_2x_3 + w_3x_4, \dots, w_1x_{n-2} + w_2x_{n-1} + w_3x_n, w_1x_{n-1} + w_2x_n) \in \mathbb{R}^n.$$

Padding also prevent the boundary elements from being treated light; without padding, x_1 and x_n contribute only once in the output while x_3, \dots, x_{n-2} appear three times.

A layer with the general form of a linear map $\mathbb{R}^n \rightarrow \mathbb{R}^m$ is said to be *fully-connected* in contrast with convolutional. We can stack convolutional and/or fully-connected layers sandwiching activation functions to form a DNN. With a fully-connected layer, we can choose arbitrary output dimension m . We have limited but some control over the size of the output of a convolutional layer. If we want to down-sample the signal, we use convolution with a *stride*. For example, with stride 2 and a padding, the output (1.1) becomes

$$(w_2x_1 + w_3x_2, w_1x_2 + w_2x_3 + w_3x_4, w_1x_4 + w_2x_5 + w_3x_6, \dots, w_1x_{n-3} + w_2x_{n-2} + w_3x_{n-1}, w_1x_{n-1} + w_2x_n) \in \mathbb{R}^{(n+1)/2}$$

when n is odd and

$$(w_2x_1 + w_3x_2, w_1x_2 + w_2x_3 + w_3x_4, w_1x_4 + w_2x_5 + w_3x_6, \dots, w_1x_{n-4} + w_2x_{n-3} + w_3x_{n-2}, w_1x_{n-2} + w_2x_{n-1} + w_3x_n) \in \mathbb{R}^{n/2}$$

when n is even. Down-sampling can also be achieved by a fixed (not learnable) filter such as the *max-pooling* and the *average-pooling* with a stride.

We can also deal with multi-channel signals. For example, for a two-channel 1D signal $x = \begin{pmatrix} x_{11}, x_{12}, \dots, x_{1n} \\ x_{21}, x_{22}, \dots, x_{2n} \end{pmatrix} \in$

$\mathbb{R}^{2 \times n}$, we use a kernel $w = \begin{pmatrix} w_{11}, w_{12}, w_{13} \\ w_{21}, w_{22}, w_{23} \end{pmatrix}$ and their convolution is

$$w * x = ((w_{11}x_{11} + w_{12}x_{12} + w_{13}x_{13}) + (w_{21}x_{21} + w_{22}x_{22} + w_{23}x_{23}), \\ (w_{11}x_{12} + w_{12}x_{13} + w_{13}x_{14}) + (w_{21}x_{22} + w_{22}x_{23} + w_{23}x_{24}), \\ \dots, (w_{11}x_{1(n-2)} + w_{12}x_{1(n-1)} + w_{13}x_{1n}) \\ + (w_{21}x_{2(n-2)} + w_{22}x_{2(n-1)} + w_{23}x_{2n})) \in \mathbb{R}^{n-2}.$$

We can also use multiple kernels to make output multi-channel; the number of output channels is equal to the number of the kernels used. For example, multiple gradient-like filters in different orientations may be useful to capture image features. With CNN's kernels (filters) are not designed by a human but learned from data. To *train* a CNN, we have to provide its objective in terms of a *loss function* (or a cost function, a energy function, a penalty function). Training means *optimising* the loss function by finding a set of weights which attains a small value of the given loss function. The training proceeds iteratively by adjusting weights gradually to lower the value of loss functions. It usually requires a lot of time and powerful equipments including GPUs.

Remark 2 A 1D signal with multiple channels shouldn't be confused with a 2D signal with a single channel. Convolution operates differently. Namely, kernels slide only spatially but not in the direction of channel.

Usually, a down-sampling layer comes with more output channels than input channels. The numbers are chosen so that the overall size of the output is smaller than that of the input and the layer serves as a compressor of information. Learning a compact representation in this manner is one of the key ideas of CNN. For 2D signals, a typical down-sampling layer has stride two with doubling output channels so that the total size is halved.

Conversely, if we want to up-sample the signal, we can for example, use simple bilinear interpolation or rearrange multiple channels [14]. Note that it has been popular to use *deconvolution* (or *transposed convolution*) for up-sampling, which is the linear adjoint to the convolution (see [13] for details). However, deconvolution often results in a draughtboard-like noise in the output [15].

Often times, between a convolution and an activation, various *normalisation* is applied for better convergence in learning [16]. In addition in image translation, normalisation is known to have a large impact on the output [17]. The popular combination of convolution followed by batch-normalisation followed by ReLU activation is abbreviated as CBR.

In image processing, the majority of neural networks are *feed forward networks* so that the data flow in one direction

and there is no feedback loop. Designing a DNN architecture mainly involves how we connect layers with different number of channels, strides, and kernel sizes.

In summary, to employ DNNs for a specific task requires

1. collecting training data (probably the hardest part)
2. designing network architecture of DNNs, loss functions (there are a variety of off-the-shelf architecture that we can just choose)
3. training (time-consuming, powerful hardware is often required).

Once a trained (learned) model, which consists of DNNs with trained weights, is obtained, just to use it is not so demanding. We only need the model and do not need the training data. The process of getting outputs from a trained model is called *inference* and it does not usually require a lot of machine power. However, it has to be noted that some information on the training data can be extracted from a trained model by a malicious attacker [18]. Therefore, a care has to be taken when we provide a learned model which is trained on data containing sensitive personal information.

1.3 Image translation with encoder-decoder networks and GANs

Now we focus on how to apply DNNs for image-to-image translation. Two powerful inventions *encoder-decoder networks* (e.g, [19]) and *generative adversarial networks (GANs)* [20] have accelerated the use of DNNs in image-to-image translation ([21]). The celebrated paper [22] crystallises how they are combined to achieve image-to-image translation, and we highly recommend the reader to have a look at it. We give an informal account of these two key ideas.

Encoder-decoder networks refers to a particular structure of DNNs which can be used to convert an input image to another. An encoder-decoder network consists of multiple down-sampling layers with increasing numbers of channels (the encoder part), followed by multiple up-sampling layers with decreasing numbers of channels (the decoder part). It has the form of an hourglass (Fig. 1). Each down-sampling layer typically reduces the image size down to a quarter, by halving in every dimension. The number of channels is usually chosen to be twice of that of the input to the layer so that the total information is compressed down to half. The purpose is to squeeze and abstract the information through the information bottleneck. The output of the middle layer is referred to as the *latent feature*. Each up-sampling layer then recovers the image size by quadrupling.

Let us consider a figurative situation to understand how this architecture works. We have two persons at both ends of a phone line. One person (the encoder) is given a bunch of noisy pictures x_1, x_2, \dots and the other (the decoder) is given

the corresponding clean pictures y_1, y_2, \dots . The encoder randomly picks $x = x_i$ and tries to describe it over the phone. Time is limited and the person cannot tell like “the left most corner has RGB value (30,41,200) and one pixel to the right has ...” but describes “there is a large house in the middle with a blue-ish roof and ...” The decoder is at the other end of the phone and tries to draw a picture y based on the explanation by the encoder. After finishing drawing, the decoder is informed of the ID of the picture, which is i , so that the decoder can compare what is drawn y with the corresponding clean picture y_i (the *ground truth*). The comparison result is fed back to the two persons to improve; the encoder improves the ability of explaining the contents of the noisy pictures, and the decoder improves drawing clean pictures from the encoder’s explanation. In the end, they are supposed to master this game and become able to restore new noisy images without ground truth. More specifically, their performance is evaluated by a *reconstruction loss function* $d(y, y_i)$ which measures the difference between two images y and y_i . A typical choice for $d(y', y_i)$ is the L^p distance between y' and y (recall that y' and y are just high dimensional vectors). In particular, the L^2 distance, which is the square root of the mean squared pixel-wise error, and the L^1 distance, which is the mean absolute pixel-wise error, are popularly used.

Through the process, visual information of the pictures are abstracted to verbal information. What is important is this abstract representation of the information. A picture with a lot of noise or with missing part can be recovered through this abstraction process. Furthermore, if we train the decoder to draw in the style of Monet, a picture is first translated into words and from words the trained painter paints like a Monet’s masterpiece. This is the basic idea of image translation using encoder-decoder networks.

But how we can train the decoder to draw like Monet? This is where the other key component GANs come into the story. If we have a lot of pairs of photos corresponding to Monet’s paintings, we can do in the same way as above with this training dataset, by giving the photos to the encoder and the corresponding paintings to the decoder. However, Monet never drew a smartphone, and the training dataset does not contain such a picture. The chance is that the encoder and the decoder cannot do good when they are asked to handle a picture of a smartphone. So we employ a third player called the *discriminator* (or the *critic*), who will be trained to distinguish real Monet’s paintings from forged ones by the decoder. The encoder and the decoder now have two separate objectives; they collaborate to convert a photo to a painting whose contents are same as in the original photo and at the same time to deceive the third player. The team of the encoder and the decoder is called the *generator*. The discriminator is trained with real paintings of Monet and generated ones and have to tell how likely a given picture is drawn by Monet. They train themselves through friendly rivalry. Their

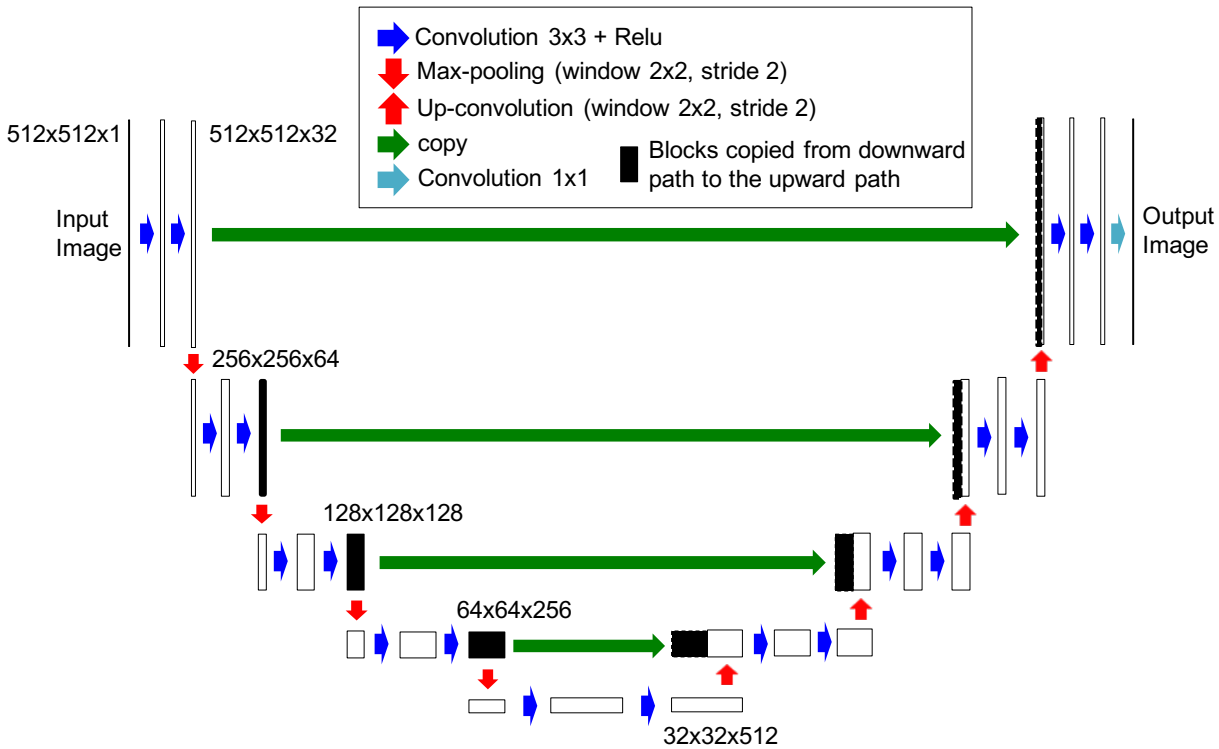


Fig. 1 Encoder-decoder network structure with skip connections (U-net), which wire the output of the first down sampling layer to the input of the last up sampling layer and similarly for the second and the penultimate, etc. The two inputs to each up sampling layers are stacked as extra channels. The idea of having skip connections is to transfer the raw, non-abstract information, especially that of high frequency signal directly to the final output. Skip connections are also useful to mitigate the *vanishing gradient problem* and accelerate learning. The 2D image size and the number of channels of the feature map from each layer were appropriately provided.

performance is evaluated in terms of the loss function. Each player is associated a tailored loss function which measures how well the player achieves its goal. A loss function is so designed that the smaller its value, the better the player is doing.

The discriminator is usually a DNN with down sampling layers whose objective and structure are same as the ones for classification tasks. The generator is an encoder-decoder network whose objective is to convert an input image with which the discriminator makes an wrong classification, and at the same time the contents of the original image is same as that of the original image. But how we can be assured that the contents of the original and the converted images are same? We can think of two different situations.

First, a *paired* images dataset consists of pairs of aligned images in the source domain A and the target domain B . For example, a photo of a cathedral and a painting of Monet of the cathedral with exactly the same angle make a paired images. We want the generator f to learn to convert $x \in A$ to $f(x) \in B$. With a paired images dataset, the discriminator will be trained to discriminate a pair (x, y) of a photo and the corresponding real painting from a pair $(x, f(x))$ of a photo and the generated painting. The discriminator's task is a classification so any classification loss can be used to

train the discriminator. The discriminator learns how Monet would paint based on a photo by optimising the discriminator's loss. It is called *conditional GAN* since the discriminator is shown the photo in addition to a forged or a real painting to judge its authenticity. The generator is given $x \in A$ and is trained to optimise a weighted sum of the *reconstruction loss* measuring the closeness between y and $f(x)$ and the *adversarial loss* which is the negative of the discriminator's loss for $(x, f(x))$. This is an instance of *supervised learning*. The idea of using conditional GAN for a general purpose image-to-image translation is extensively investigated in *pix2pix* [22]. However, paired images are hard to acquire in medical imaging, as the images must be aligned almost perfectly to make paired images.

On the other hand, an *unpaired* image dataset consists of a set of images from the source domain A and an independent set of images from the target domain B . We do not know which image in A corresponds to which in B . Again, we want the generator f to learn to convert $x \in A$ to $f(x) \in B$. The discriminator is trained to distinguish real images y from generated images $f(x)$. Note that here y and x here are independent and do not correspond to each other; y could be a painting of water lily while x is a smartphone. In this case, it is difficult to preserve the contents under transla-

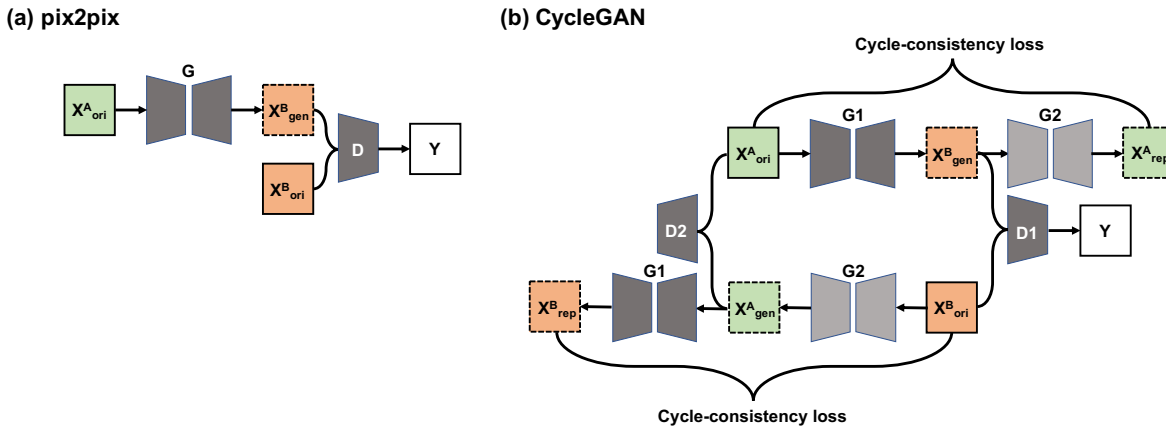


Fig. 2 The architecture of (a) pix2pix and (b) CycleGAN. (a) pix2pix requires perfectly aligned paired training images. A generator CNN is trained to generate images similar to images in domain B from images in domain A and discriminator CNN is trained simultaneously to distinguish the generated images from real images in domain B . Reconstruction loss which measures how close the real images in domain B and the generated images in addition to adversarial loss are optimized. On the other hands, (b) CycleGAN can learn a translation mapping in the absence of aligned paired images. The images generated from domain A to domain B by generator CNN ($G1$) is converted back to domain A by another generator CNN ($G2$), and vice versa, trying to optimise the cycle-consistency in addition to adversarial loss.

tion, as the encoder and the decoder have no way to check if the decoder’s drawing corresponds to what the encoder describes. That is, it is difficult to define a reconstruction loss as we do not have the ground truth on what $f(x)$ should be. One trick to encourage the content preservation is to introduce another group of a generator g and a discriminator, who are trained to convert in the opposite direction from the target domain B to the source domain A . We demand that a converted image by the first group is converted back to the original, and vice versa. That is, the *cycle-consistency loss* $|x - g(f(x))|^2 + |y - g(f(y))|^2$ should also be optimised. This encourages both parties to learn one-to-one mappings. The architecture of the whole system is depicted in Figure 2. This is an instance of *unsupervised learning*. The cycle-consistency loss is introduced in *CycleGAN* [23]³. This does not guarantee the contents preservation, though. So we have to be careful when using CycleGAN. Anatomical structures can be altered and non-existing tumors can be made up in the converted images. To further encourage the structure preservation, the perceptual loss (or the content loss) between the original and the converted image can be added as an optimisation target of the generators. The perceptual loss between two images x and y is defined to be $|h(x) - h(y)|^2$, where h is another DNN pretrained on natural images (typically, the VGG19 network trained on the ImageNet dataset truncated just before the fully-connected layer is used for f). The idea is to compare the high-level, abstract features of images extracted by a pretrained DNN; DNNs trained with natural

images are like human eyes. The perceptual loss is generally useful when a direct pixel-by-pixel comparison does not make sense (e.g., when images contain strong noise).

Obviously, it is better to use pix2pix than CycleGAN when a paired image dataset is available (see [23] for comparison study). However, in case the alignment of paired images are not perfect, CycleGAN may perform better.

With this purely data driven approach, any image-to-image translation tasks go almost in the same manner. Only different sets of data consisting of task specific images are required. In fact, AUTOMAP [26] demonstrated the ubiquity of this approach in a medical setting by showing the same network can be used for reconstruction of PET, CT, and MRI. They rely on encoder-decoder network and does not use GANs. What is special with reconstruction is that the spatial correspondence between the original and the reconstructed images are not straightforward. The fundamental assumption behind convolutional neural networks is that spatially close pixels are highly correlated so that convolution with a small kernel such as 3×3 captures meaningful features. On the other hand, adjacent pixels, say in the frequency domain as in MRI, do not necessarily affect neighbouring pixels in the reconstructed image. The novel idea of AUTOMAP is to use a few fully-connected layers *before* a typical convolutional encoder-decoder network. The fully-connected layers are supposed to learn mathematical transformations such as (inverse) Fourier transformation and Radon transformations, which require spatially non-local manipulation.

Remark 3 One popular variant of the encoder-decoder networks called the *U-Net* [19] uses *skip connections* which wire the output of the first down sampling layer to the input of the last up sampling layer and similarly for the second and

³ Around the same time, very similar architectures such as UNIT, DiscoGAN, and DualGAN were introduced. Walender et al. [24] evaluated UNIT [25] and CycleGAN for transformation between T1 and T2-weighted MRI images and showed that these two frameworks performed almost equally well.

the penultimate, etc. The two inputs to each up sampling layers are stacked as extra channels. The idea is to transfer the raw, non-abstract information, especially that of high frequency signal directly to the final output. Skip connections are also useful to mitigate the *vanishing gradient problem* and accelerate learning.

Remark 4 GANs are notoriously difficult to train, as the balance among different players is required. Several techniques are known for a stable training such as Wasserstein GAN with gradient penalty (WGAN-GP) [27], Progressive Growing GAN (PGGAN) [28], and spectral normalization [29].

2 Noise reduction

Noise reduction is the process of removing noise in the images acquired through imaging, typically those with low-dose CT (LDCT). It can be considered as translating an image with noise to one with reduced noise. Among model based approaches, iterative reconstruction (IR) with some kinds of prior information has been used for the reduction of noise and artifact. However, its slow reconstruction speed and its output quality have limited its clinical application. Recently, denoising method using deep neural networks (DNN) have been intensively studied (see [30]). Most of the DNN-based method are post-processing of reconstructed images, which does not rely on raw projection data. For simplicity, we focus on the setting of denoising LDCT in order to obtain a image resembling normal-dose CT (NDCT). The same techniques work for other scenario straightforwardly.

Chen et al. [31] proposed a shallow encoder-decoder network trained with a paired dataset consisting of NDCT images and LDCT images. Here, NDCT images are acquired routinely and the LDCT images are artificially generated by adding Poisson noise to the corresponding NDCT images. The end-to-end mapping from LDCT images to NDCT images was learned using the DNN. Once trained, the network takes LDCT images as input and converts it to one similar to NDCT images. The output quality is less plausible when compared with that of the state-of-the-art algorithms which we review later in this subsection. However, their paper is simple and well-written and good for grasping the basic ideas on denoising with DNNs. Although this simple method greatly reduce the noise of LDCT images, a limitation is that the result images look over-smoothed and lose structure details sometimes since these methods targets minimizing only reconstruction losses between NDCT images and converted NDCT-like images in the training dataset and do not generalise well for new unseen images. One solution to this problem is to use GAN based methods such as pix2pix. As we discussed in the previous section, pix2pix requires perfectly aligned paired training images, which may

be difficult to obtain in clinical settings. There are mainly two ways to prepare such paired datasets.

- Noisy images are created by adding artificial noise to high-quality NDCT images. The problem with this method is that the noise distribution is different from the real one.
- Multiple acquisition are performed at different dose. The problem with this method is that the images are not perfectly aligned even if they are registered with DIR (deformable image registration).

With a paired dataset at hand, a generator DNN is trained to generate NDCT-like images from LDCT images trying to optimise a reconstruction loss which measures how close the real NDCT images and the generated NDCT-like images. A discriminator CNN was trained simultaneously to distinguish the generated NDCT-like images from real NDCT images. The generator tries to produce NDCT-like images which fool the discriminator by optimising the adversarial loss in addition to the reconstruction loss. For a reconstruction loss, the squared sum of pixel-wise difference in value (the squared L^2 loss) is often used, but it results in blurry outputs. Alternative loss functions include the perceptual feature loss [32], the *structure loss* [33], and *sharpness loss* [34] have been investigated. Any of these loss functions is dependent on the accuracy of the alignment of paired images, and aligned paired training images are indispensable to use pix2pix framework. However, in real clinical situation, aligned paired LDCT and NDCT images are difficult to obtain. Creating LDCT by adding artificial noise to NDCT images has a problem of difference from actual noise of LDCT, and multiple acquisition at different dose has problems of additional radiation dose to patients and position errors between acquisitions.

On the other hand, CycleGAN can learn a translation mapping in the absence of aligned paired images. Kang et al [35] applied CycleGAN to learn the mapping between the low- and normal- dose cardiac phases, which are not aligned to each other exactly due to the cardiac motion. Their method effectively reduces the noise in the low dose cardiac images while suppressing the deformation and loss of structures.

3 Super resolution

The purpose of super resolution (SR) is recovering a high-resolution image from a single low-resolution image. Most of existing methods for SR learn mapping functions from external low- and high-resolution example pairs (paired dataset). Conventional SR methods learn the dictionaries [36,37] or manifolds [38,39] for modeling the patch space. On the other hand, DNN based methods learn an end-to-end mapping between low- and high-resolution images, so implicitly achieved dictionaries or mapping functions for patch space by hidden layers of DNN. With SRCNN (Super-Resolution Con-

volutional Neural Network), low-resolution input images are first upsampled to the desired size using bicubic interpolation and then fed to an encoder-decoder network, thus end-to-end mapping between bicubic upsampled version of low-resolution image and ground truth high-resolution image is learned. The SRCNN has been applied to Mammography images [40], Chest CT images [41] and MRI images [42].

SRGAN (Super-Resolution Using a Generative Adversarial Network) [43] can be seen as a GAN-fortified version of SRCNN. An encoder-decoder network with more upsampling layers than downsampling layers is trained to recover detailed textures from heavily downsampled images, and a discriminator is trained to differentiate between the super-resolved images and original high-quality images. SRGAN has been applied to generate high-resolution brain MRI images from low-resolution images and 3D convolutions has been adopted to exploit volumetric information [44].

4 Image synthesis

Medical image synthesis is performed for two purposes. One of which is to expand a small dataset with new, plausible examples for training of DNNs for diagnosis and other tasks. The other is to generate images virtually which are not acquired due to the clinical workflow or reduction of the acquisition time, cost and dose. For the former purpose, transformation such as shifts, flips, zooms, rotations have been performed traditionally. However, enough variations in size, shape and contrast of samples cannot be obtained, which result in the deterioration of the accuracy of detection and classification task. To cope with this problem, unconditional synthesis using GAN, which generate images from noise without any other conditional information, has been performed for generating various plausible training images [45,46,47,48,50]. For the latter purpose, cross modality synthesis such as generating CT-like image from MRI image using GAN has been proposed [56,57,59]. The CT-like images synthesized from MRI images may be applied to dose calculation (treatment planning) for upcoming MRI-only radiotherapy.

4.1 Unconditional synthesis

Unconditional synthesis using GAN generate images from noise without any other conditional information. It can be considered as image-to-image translation in which input images are just randomly generated noise. Deep convolutional GAN (DCGAN) and its improved variant Progressive Growing of GAN (PGGAN) have been used for generation of medical images. DCGAN have been used to generate synthetic samples of CT images of lung nodule [45] and liver lesion [46], MRI images of brain [47] and X-ray images of chest [48]. PGGAN have been used to generate synthetic

samples of Mammography images [50]. It is noted that DCGAN have been applied to an image resolution of up to 256×256 but PGGAN can be applied to an image resolution of up to 1024×1024 . The key idea of PGGAN is to grow both the generator and discriminator progressively: starting from a low resolution and new layers that model increasingly fine details as training progresses are added.

These GAN-based augmented images were found to be beneficial to various classification and segmentation tasks when combined with real images. Wu et al. [60] reported that a GAN-based augmentation improved Area Under the Curve (AUC) of mammogram patch-based classification by 0.009 ($0.887 \rightarrow 0.896$) over a traditional augmentation approach. Mok et al. [51] reported that a PGGAN-based augmentation improved the dice coefficient of segmentation of brain tumor by 0.03 ($0.81 \rightarrow 0.84$) over a traditional augmentation approach. Frid-Adar et al. [49] reported that a DCGAN-based augmentation improved the classification of liver lesion by 7.1% ($78.6\% \rightarrow 85.7\%$) in sensitivity and 4.0% ($88.4\% \rightarrow 92.4\%$) in specificity over a traditional augmentation approach.

4.2 Cross modality synthesis

Cross-modality synthesis using encoder-decoder networks has been explored in several works, which include MRI-to-CT synthesis [52,53] and Cone beam CT-to-Planning CT synthesis [54]. In case images from two different modalities can be spatially aligned correctly such as PET-CT, where PET images and CT images are acquired simultaneously [55], pix2pix can be used. On the other hand, CycleGAN is used in case it is clinically difficult or impossible to acquire aligned paired training images from two different modalities such as CT and MRI images, which are acquired with different modality on different timing [56,57,59].

Wolterink et al. [56] synthesize CT images of the head from MRI images of the head using CycleGAN, and they also showed that CycleGAN using unpaired images created CT images looked more realistic and contained less artifacts and blurring than GAN combined with voxel-wise loss using aligned images. The difference could be due to misalignment between MRI and CT images, which is ignored when training with unpaired images using CycleGAN. However, CycleGAN sometimes fail to preserve the boundary of structures when using the images such as pelvic region, which has large variation of the anatomical structures between images from two different modalities due to the presence of joints, muscles, intestines, rectums. Hiasa et al. [57] extended CycleGAN by incorporating gradient consistency loss to preserve the boundary of structures in pelvic region at MRI-to-CT synthesis. They showed that synthesized images with gradient consistency loss preserved better the shape

	Encoder-decoder	pix2pix	CycleGAN	UNIT	SRCNN	SRGAN	DCGAN	PGGAN
Noise-reduction	[31]	[32] [33] [34]	[35]					
Super-resolution					[40] [41] [42]	[43] [44]		
Unconditional synthesis							[45] [46] [47] [48] [49]	[50] [51]
Cross modality synthesis	[52] [53] [54]	[55]	[56] [57] [58] [59] [24]	[25] [24]				

Table 1 A brief summary of tasks and networks in the reviewed publications

near the femoral head and adductor muscles than those without gradient consistency loss. Kida et al. [58] also extended CycleGAN by incorporating several losses for better preservation of the boundary of structures in pelvic region at Cone beam CT-to-Planning CT synthesis. They showed that edge sharpness and structures were preserved in not only large bulky tissues such as rectum and bladder but also small isolated structures as small intestine and intestinal gas. It is noted that they showed with some initial weightings, the generators completely failed to learn a good mapping and produced totally distorted images. This kind of failure tends not to be reported but practitioners have to be warned when planning to deploy DNN-based methods. Zhang et al. [59] employed shape consistency loss that is produced by another image-to-image translation DNN for segmentation named the segmentor. One segmentor is introduced to each domain to learn segmentation, in addition to the generator and the discriminator. The segmentor’s outputs for the original and the translated images are compared in the shape consistency loss, which encourages the generator not to alter the semantics. This is a type of a perceptual loss. During training, the segmentor takes advantage of the generator by using synthetic images as augmented data, and the generator and the segmentor prompt each other through the loss functions. Finally, the segmentors provide implicit shape constraints on the anatomy structures during image synthesis. It is noted that semantic labels (annotated segmentation) of training images from both modalities are required.

5 Reconstruction

Imaging such as CT, MRI, and PET can also be thought of as a specific instance of image-to-image translation from a volumetric object (density distribution) in the three dimensional space to a (series of) projection image(s). In other words, imaging is a mapping

$$Im : \mathbb{R}^{d_1 \times h_1 \times w_1} \rightarrow \mathbb{R}^{d_2 \times h_2 \times w_2}.$$

Reconstruction is then the translation from the projection image back to the original distribution and is regarded as a mapping

$$Rec : \mathbb{R}^{d_2 \times h_2 \times w_2} \rightarrow \mathbb{R}^{d_1 \times h_1 \times w_1}$$

so that $Rec \circ Im$ is the identity. In the ideal setting of no noise and infinite resolution, mathematics allows us to find a good

reconstruction mapping Rec for each imaging mapping Im such as the filtered back-projection for fan-beam CT. However, the reality is that we have to tackle with technical difficulties such as noise and low resolution due to scanner and dose limitation, and numerical error of the algorithm. In this section, we discuss what machine learning can offer for an improved reconstruction.

5.1 Hybrid approach

As reconstruction can be thought of as image-to-image translation, DNNs discussed in §1.3 (e.g., AUTOMAP [26]) can be directly applicable if we have enough data consisting of pairs of original and translated images. That is, we can approximate the reconstruction mapping by a DNN. Purely data driven methods do not rely on the fact that imaging is the result of a physical process subject to certain rules. Here, we see how we can exploit the knowledge from physics and mathematics, and combine it to data driven approaches to enhance the performance. In this way, we will achieve a better quality reconstruction with less amount of training image pairs.

Most of imaging techniques guarantee at least theoretically that for each projection there exists a unique distribution so the projection and the original distribution contain exactly same amount of information. However, due to the noise and the finite resolution, some information gets lost under the imaging process, which makes the reconstruction *ill-posed* and difficult. That is, given a projection image, we cannot expect to find one and only distribution which projects to the projection image. Therefore, the aim of reconstruction is to find a distribution which translates as closely as possible to the given projection with respect to some goodness and closeness criteria.

In practice, we (assume to) know the mathematical model of the imaging, which is represented by

$$y = Im(x), \tag{5.1}$$

where x is a distribution, y is the corresponding projection. The imaging mapping Im is often called the *forward operator* and is determined by the configuration of the imaging equipment such as the scanner geometry and the sub-sampling scheme. If Im were invertible, we can directly solve $x = Im^{-1}(y)$, but usually the equation (5.1) is ill-posed due to the hardware limitations and there is no Im^{-1} . Therefore, reconstruction takes the form of an optimisation problem;

namely, we would like to find x^* which minimises the following

$$L(x) = d(y, Im(x)) + \lambda E(x), \quad (5.2)$$

where the *reconstruction loss term* (or the *data fidelity term*) $d(y, Im(x))$ tells how close y and $Im(x)$ are, the *regularisation term* $E(x)$ tells how appropriate x is as a reconstructed image, and $\lambda > 0$ determines the balance between the two criteria. Such x^* is often denoted by $\text{argmin}(L(x))$. There are many choices for d , E , and λ . Once we fix Im , d , E , and λ , all we have to do for the reconstruction is simply optimising (find x which attain the small value of) (5.2). The reader may notice that this is exactly same as the formulation of iterative reconstruction.

Popular choices for d are the L^1 norm and the L^2 norm. Both are just standard distances in the Euclidean space. While L^2 penalises large deviation in values a lot, it is permissive for small deviation in a large region. This characteristics often leads to a blurry output. On the other hand, L^1 prefers two images to be exactly same at most of pixels but allow the rest to deviate a lot. It is good to keep this intuition in mind to design loss functions tailored for specific applications. We can also use a DNN for d measuring an abstract distance between images such as a perceptual loss (see §1.3).

The purpose of the regularisation term is three-fold:

1. to incorporate prior for a higher quality output
2. to suppress over-fitting for a better generalisation
3. to mitigate ill-posedness for a better convergence of the optimisation

For example, it is reasonable to ask for a solution image which has some spatial uniformity. A popular conventional choice is the L^1 -norm of the image gradient (total variation). We can also use DNNs to learn image priors from data [61]. The idea is similar to GANs; a DNN is trained with the images in the reconstructed domain to learn their distribution. In fact, we can use the adversarial loss from a discriminator trained with high-quality reconstructed images and images x which are in the middle of reconstruction. One problem, however, is that such high-quality images may not be available as we have no way to know the ground truth distribution of our body except for phantoms. Therefore, the method is useful when we have high-quality reconstruction images (e.g., planning CT) and we want to do reconstruction with limited quality projections (low-dose CT). The regularisation term E can consist of many sub-terms. For example, we can take E to be a weighted sum of the total variation and the adversarial loss.

Another interesting way of regularisation called the deep image prior is proposed in [62], which does not take the form of the added term E . Instead, the idea is to replace x with $f_w(0)$ in (5.2), where f is a DNN with weights w . The optimisation is performed not directly on x but indirectly

on w . One way to understand this is to think of DNNs as a restricted approximator of arbitrary signals, just as trigonometric functions and wavelet functions are conventionally used to approximate signals x . We know from sparse modelling that if we restrict ourselves to use only a small number of them, we obtain better results. As DNNs are suitable to represent visual information which our eyes can perceive, it may be more reasonable to use DNNs rather than trigonometric functions and wavelets as an approximator. In other words, while x can take any value in the whole Euclidean space, $f_w(0)$ is constrained within the image of a mapping $w \mapsto f_w(0)$, which are more likely to be visually plausible.

In any case, the motto of regularisation is “do not give a complete freedom, but restrict in a reasonable manner” as in ordinary education.

In view of the optimisation of (5.2), both model based and data driven approaches are integrated. This hybrid approach is studied actively in recent years (see, for example, [63,61,64]).

Image-to-image translation by DNNs reviewed in the previous sections can be seen as replacing the whole process of the optimisation of (5.2) by DNNs which directly find x_* from given inputs y .

6 Sample codes

In this section, we give a hands-on account on what we encounter in deployment of DNNs in a specific task. We use our codes for image-to-image translation for both paired and unpaired dataset, which would cover most of the topics in the article except for those in §5.1. Our codes are written in Python using a deep learning framework Chainer [65]. For a demonstration purpose, we work on a simple denoising scenario, where we assume that a high-quality training dataset is available. For other image-to-image translation tasks, the workflow is more or less same except how datasets are acquired. Note that the purpose of the section is to give an overview on how an actual procedure may look, and we do not mean to make a practical denoising model.

For DNNs, we use our code available at [3] for general image-to-image translation DNNs for paired datasets. How to setup the running environment and what to type to run the code are instructed in the code’s documentation.

For datasets, we use CPTAC-SAR [66], which is made publicly available at The Cancer Imaging Archive. The dataset contains normal-dose CT images of Sarcomas cohort in the DICOM format. We make low-quality noisy CT images by adding artificial Poisson noise. This is done by the python script included in [3] as instructed in the documentation. Now, we have hundreds of pairs of a noisy and a clean CT images, and we train a DNN based on pix2pix to learn a mapping from a noisy image to a clean one. During the training, the dataset is *augmented* on the fly by random crop and

flip, and by adding random Gaussian noise. There are numerous *hyper-parameters* for training;

- how long (how many *epochs*) the training lasts; recall that training is an optimisation, and the user has to decide when to stop.
- how many layers the encoder-decoder network and the discriminator network have; network architectures have to be fixed
- how to weight different loss functions

just to mention a few. The code comes with reasonable default values for them, but to get the best performance, the user has to *tune* them depending on the dataset and the goal of the task. Basically, we search by trial and error to find the best hyper-parameter setting. One training takes from hours to days, so tuning can be very time consuming.

Once we obtain a well-trained model, we can use it to denoise new DICOM images. It can process dozens of images per second even without a GPU. The trained model may or may not *generalise* to images obtained somewhere else. DNNs basically learn how to handle with images which are similar to those in the training dataset. New images can have totally different noise characteristics, or contain different organs. When the trained model's performance is not satisfactory, we have to find other datasets and/or modify network architecture, and/or tune hyper-parameters until satisfied.

This is a typical procedure of deploying DNNs in an image processing task. We can also use [2] to work with an unpaired dataset e.g., with noisy images from one patient and clean images from another.

7 Conclusion

In recent years, use of DNNs is getting dominant in medical image processing. A lot of tasks are considered as instances of image-to-image translation. Two key inventions encoder-decoder networks and GANs have improved the usability of DNNs in image-to-image translation, and there are two fundamental architectures utilising them; pix2pix and CycleGAN. They are used for different types of dataset; pix2pix is preferable when a dataset consisting of paired images is available, while CycleGAN can work with a dataset consisting of unpaired images. The following table summarises various medical applications we reviewed in this paper in terms of their base architectures (Tab. 4).

In some cases conventional model based approaches do better than DNNs especially when the available data are limited. Also, data driven approaches often lack in explainability, and we may get totally wrong outputs for certain inputs. Thus, to quantify uncertainty and to establish evaluation and validation scheme is crucial for the reliable deployment in clinical applications. They are among the high priority research topics in machine learning (e.g., [67]).

We would like to emphasise that we have to be careful when using DNN-based methods, however, at the same time, we must not be extremely afraid of using DNNs. After all, they are merely tools. As long as the user knows its proper usage and limitations, they are an extreme powerful companion for practitioners in clinical medicine. It is like spelling helpers for authors. We have written this article with a word processor with a spelling helper. It corrects spelling automatically, but sometimes it makes mistakes. Nevertheless, the number of corrected words are much bigger than that of mis-corrected. We just should not have trusted it completely, but had to check the words again by ourselves.

For each medical image processing scenario, the best method should be a hybrid combining the advantages from both data driven and model based approaches, incorporating domain specific knowledge to DNNs. Some programming frameworks have been developed to enable hybrid approaches relatively easy. For example, ODL [68] is a python-based framework for reconstruction algorithms which is integrated with deep learning frameworks. For innovative advancements, radiologists, physicists, mathematicians, and computer scientists have to team up and conduct interdisciplinary research.

References

1. B. Sahiner, A. Pezeshk, L. M. Hadjiiski, X. Wang, K. Drukker, K. H. Cha, R. M. Summers, and M. L. Giger, "Deep learning in medical imaging and radiation therapy.," *Medical physics*, 2018.
2. S. Kaji, "Image translation by CNNs trained on unpaired data." <https://github.com/shizuo-kaji/UnpairedImageTranslation>, 2019.
3. S. Kaji, "Image translation for paired image datasets (automap + pix2pix)." <https://github.com/shizuo-kaji/PairedImageTranslation>, 2019.
4. L. Lu, Y. Zheng, G. Carneiro, and L. Yang, eds., *Deep Learning and Convolutional Neural Networks for Medical Image Computing - Precision Medicine, High Performance and Large-Scale Datasets*. Advances in Computer Vision and Pattern Recognition, Springer, 2017.
5. F. Knoll, A. K. Maier, and D. Rueckert, eds., *Machine Learning for Medical Image Reconstruction - First International Workshop, MLMIR 2018, Held in Conjunction with MICCAI 2018, Granada, Spain, September 16, 2018, Proceedings*, vol. 11074 of *Lecture Notes in Computer Science*, Springer, 2018.
6. G. J. S. Litjens, T. Kooi, B. E. Bejnordi, A. A. A. Setio, F. Ciompi, M. Ghahfoorian, J. van der Laak, B. van Ginneken, and C. I. Sánchez, "A survey on deep learning in medical image analysis.," *Medical image analysis*, vol. 42, pp. 60–88, 2017.
7. J. Schindelin, I. Arganda-Carreras, E. Frise, V. Kaynig, M. Longair, T. Pietzsch, S. Preibisch, C. Rueden, S. Saalfeld, B. Schmid, J.-Y. Tinevez, D. J. White, V. Hartenstein, K. Eliceiri, P. Tomancak, and A. Cardona, "Fiji: an open-source platform for biological-image analysis.," *Nat Meth*, vol. 9, pp. 676–682, July 2012.
8. M. A. Nielsen, "Neural networks and deep learning.," 2018.
9. I. J. Goodfellow, Y. Bengio, and A. Courville, *Deep Learning*. Cambridge, MA, USA: MIT Press, 2016. <http://www.deeplearningbook.org>.

10. I. Safran and O. Shamir, "Depth-width tradeoffs in approximating natural functions with neural networks," in *Proceedings of the 34th International Conference on Machine Learning - Volume 70, ICML'17*, pp. 2979–2987, JMLR.org, 2017.
11. F. Scarselli and A. C. Tsoi, "Universal approximation using feed-forward neural networks: A survey of some existing methods, and some new results," *Neural Netw.*, vol. 11, pp. 15–37, Jan. 1998.
12. Z. Lu, H. Pu, F. Wang, Z. Hu, and L. Wang, "The expressive power of neural networks: A view from the width," in *Advances in Neural Information Processing Systems 30* (I. Guyon, U. V. Luxburg, S. Bengio, H. Wallach, R. Fergus, S. Vishwanathan, and R. Garnett, eds.), pp. 6231–6239, Curran Associates, Inc., 2017.
13. V. Dumoulin and F. Visin, "A guide to convolution arithmetic for deep learning," 2016. arXiv:1603.07285.
14. W. Shi, J. Caballero, F. Huszar, J. Totz, A. P. Aitken, R. Bishop, D. Rueckert, and Z. Wang, "Real-time single image and video super-resolution using an efficient sub-pixel convolutional neural network," in *2016 IEEE Conference on Computer Vision and Pattern Recognition, CVPR 2016, Las Vegas, NV, USA, June 27-30, 2016*, pp. 1874–1883, 2016.
15. A. Odena, V. Dumoulin, and C. Olah, "Deconvolution and checkerboard artifacts," *Distill*, 2016.
16. S. Ioffe and C. Szegedy, "Batch normalization: Accelerating deep network training by reducing internal covariate shift," in *ICML (F. R. Bach and D. M. Blei, eds.)*, vol. 37 of *JMLR Workshop and Conference Proceedings*, pp. 448–456, JMLR.org, 2015.
17. D. Ulyanov, A. Vedaldi, and V. S. Lempitsky, "Improved texture networks: Maximizing quality and diversity in feed-forward stylization and texture synthesis," in *2017 IEEE Conference on Computer Vision and Pattern Recognition, CVPR 2017, Honolulu, HI, USA, July 21-26, 2017*, pp. 4105–4113, 2017.
18. M. Fredrikson, S. Jha, and T. Ristenpart, "Model inversion attacks that exploit confidence information and basic countermeasures," in *Proceedings of the 22nd ACM SIGSAC Conference on Computer and Communications Security, CCS '15, (New York, NY, USA)*, pp. 1322–1333, ACM, 2015.
19. O. Ronneberger, P. Fischer, and T. Brox, "U-net: Convolutional networks for biomedical image segmentation," in *Medical Image Computing and Computer-Assisted Intervention - MICCAI 2015 - 18th International Conference Munich, Germany, October 5 - 9, 2015, Proceedings, Part III*, pp. 234–241, 2015.
20. I. Goodfellow, J. Pouget-Abadie, M. Mirza, B. Xu, D. Warde-Farley, S. Ozair, A. Courville, and Y. Bengio, "Generative adversarial nets," in *Advances in Neural Information Processing Systems 27* (Z. Ghahramani, M. Welling, C. Cortes, N. D. Lawrence, and K. Q. Weinberger, eds.), pp. 2672–2680, Curran Associates, Inc., 2014.
21. X. Yi, "Awesome GAN for medical imaging." <https://github.com/xinario/awesome-gan-for-medical-imaging>, 2019.
22. P. Isola, J. Zhu, T. Zhou, and A. A. Efros, "Image-to-image translation with conditional adversarial networks," in *2017 IEEE Conference on Computer Vision and Pattern Recognition, CVPR 2017, Honolulu, HI, USA, July 21-26, 2017*, pp. 5967–5976, 2017.
23. J. Zhu, T. Park, P. Isola, and A. A. Efros, "Unpaired image-to-image translation using cycle-consistent adversarial networks," in *IEEE International Conference on Computer Vision, ICCV 2017, Venice, Italy, October 22-29, 2017*, pp. 2242–2251, 2017.
24. P. Welander, S. Karlsson, and A. Eklund, "Generative adversarial networks for image-to-image translation on multi-contrast MR images - A comparison of CycleGAN and UNIT," 2018. arXiv:1806.07777.
25. M.-Y. Liu, T. Breuel, and J. Kautz, "Unsupervised image-to-image translation networks," in *Advances in Neural Information Processing Systems 30* (I. Guyon, U. V. Luxburg, S. Bengio, H. Wallach, R. Fergus, S. Vishwanathan, and R. Garnett, eds.), pp. 700–708, Curran Associates, Inc., 2017.
26. B. O. Zhu, J. Z. Liu, B. R. Rosen, and M. S. Rosen, "Image reconstruction by domain-transform manifold learning," *Nature*, vol. 555, pp. 487–492, 2018.
27. I. Gulrajani, F. Ahmed, M. Arjovsky, V. Dumoulin, and A. C. Courville, "Improved training of Wasserstein GANs," in *Advances in Neural Information Processing Systems 30* (I. Guyon, U. V. Luxburg, S. Bengio, H. Wallach, R. Fergus, S. Vishwanathan, and R. Garnett, eds.), pp. 5767–5777, Curran Associates, Inc., 2017.
28. T. Karras, T. Aila, S. Laine, and J. Lehtinen, "Progressive growing of GANs for improved quality, stability, and variation," in *6th International Conference on Learning Representations, ICLR 2018, Vancouver, BC, Canada, April 30 - May 3, 2018, Conference Track Proceedings*, 2018.
29. T. Miyato, T. Kataoka, M. Koyama, and Y. Yoshida, "Spectral normalization for generative adversarial networks," in *6th International Conference on Learning Representations, ICLR 2018, Vancouver, BC, Canada, April 30 - May 3, 2018, Conference Track Proceedings*, 2018.
30. J. Sinyu, "CT image denoising with deep learning." https://github.com/SSinyu/CT_DENOISING_REVIEW, 2018.
31. H. Chen, Y. Zhang, W. Zhang, P. Liao, K. Li, J. Zhou, and G. Wang, "Low-dose CT via convolutional neural network," *Biomed. Opt. Express*, vol. 8, pp. 679–694, Feb 2017.
32. Q. Yang, P. Yan, Y. Zhang, H. Yu, Y. Shi, X. Mou, M. K. Kalra, Y. Zhang, L. Sun, and G. Wang, "Low-dose CT image denoising using a generative adversarial network with Wasserstein distance and perceptual loss," *IEEE Transactions on Medical Imaging*, vol. 37, pp. 1348–1357, June 2018.
33. C. You, Q. Yang, H. Shan, L. Gjestebj, G. Li, S. Ju, Z. Zhang, Z. Zhao, Y. Zhang, W. Cong, and G. Wang, "Structurally-sensitive multi-scale deep neural network for low-dose CT denoising," *IEEE Access*, vol. 6, pp. 41839–41855, 2018.
34. X. Yi and P. Babyn, "Sharpness-aware low-dose CT denoising using conditional generative adversarial network," *Journal of Digital Imaging*, vol. 31, pp. 655–669, Oct 2018.
35. E. Kang, H. J. Koo, D. H. Yang, J. B. Seo, and J. C. Ye, "Cycle-consistent adversarial denoising network for multiphase coronary CT angiography," *Medical Physics*, vol. 46, pp. 550–562, Feb. 2019.
36. R. Timofte, V. D. Smet, and L. V. Gool, "Anchored neighborhood regression for fast example-based super-resolution," *2013 IEEE International Conference on Computer Vision*, pp. 1920–1927, 2013.
37. J. Yang, J. N. Wright, T. S. Huang, and Y. Ma, "Image super-resolution as sparse representation of raw image patches," *2008 IEEE Conference on Computer Vision and Pattern Recognition*, pp. 1–8, 2008.
38. M. Bevilacqua, A. Roumy, C. Guillemot, and M.-L. Alberi-Morel, "Low-complexity single-image super-resolution based on nonnegative neighbor embedding," in *BMVC*, 2012.
39. H. Chang, D.-Y. Yeung, and Y. Xiong, "Super-resolution through neighbor embedding," *Proceedings of the 2004 IEEE Computer Society Conference on Computer Vision and Pattern Recognition, 2004. CVPR 2004.*, vol. 1, pp. I–I, 2004.
40. T. I. Kensuke Umehara, Junko Ota, "Super-resolution imaging of mammograms based on the super-resolution convolutional neural network," *Open Journal of Medical Imaging*, vol. 7, pp. 180–195, 2017.
41. K. Umehara, J. Ota, and T. Ishida, "Application of super-resolution convolutional neural network for enhancing image resolution in chest ct," *J Digit Imaging*, pp. 180–195, 2017.
42. E. Plenge, D. H. J. Poot, M. Bernsen, G. Kotek, G. Houston, P. Wielopolski, L. van der Weerd, W. J. Niessen, and E. Meijering, "Super-resolution methods in MRI: Can they improve the trade-off between resolution, signal-to-noise ratio, and acquisition time?," *Magn Reson Med*, vol. 68, pp. 1983–1993, 2012.

43. C. Ledig, L. Theis, F. Huszar, J. Caballero, A. Cunningham, A. Acosta, A. P. Aitken, A. Tejani, J. Totz, Z. Wang, and W. Shi, "Photo-realistic single image super-resolution using a generative adversarial network," in *CVPR*, pp. 105–114, IEEE Computer Society, 2017.
44. I. Sánchez and V. Vilaplana, "Brain MRI super-resolution using generative adversarial networks," in *International Conference on Medical Imaging with Deep Learning*, (Amsterdam, The Netherlands), 07/2018 2018.
45. M. J. M. Chuquicuma, S. Hussein, J. R. Burt, and U. Bagci, "How to fool radiologists with generative adversarial networks? a visual Turing test for lung cancer diagnosis," *2018 IEEE 15th International Symposium on Biomedical Imaging (ISBI 2018)*, pp. 240–244, 2018.
46. M. Frid-Adar, I. Diamant, E. Klang, M. Amitai, J. Goldberger, and H. Greenspan, "GAN-based synthetic medical image augmentation for increased CNN performance in liver lesion classification," *Neurocomputing*, vol. 321, pp. 321–331, 2018.
47. C. Bermudez, A. J. Plassard, L. T. Davis, A. T. Newton, S. M. Resnick, and B. A. Landman, "Learning implicit brain MRI manifolds with deep learning," *Proceedings of SPIE—the International Society for Optical Engineering*, vol. 10574, 2018.
48. A. Madani, M. Moradi, A. Karargyris, and T. Syeda-Mahmood, "Chest x-ray generation and data augmentation for cardiovascular abnormality classification," 2018.
49. M. Frid-Adar, E. Klang, M. Amitai, J. Goldberger, and H. Greenspan, "Synthetic data augmentation using GAN for improved liver lesion classification," *2018 IEEE 15th International Symposium on Biomedical Imaging (ISBI 2018)*, pp. 289–293, 2018.
50. D. Korkinof, T. Rijken, M. O'Neill, J. Yearsley, H. Harvey, and B. Glocker, "High-resolution mammogram synthesis using progressive generative adversarial networks," 2018. arXiv:1807.03401.
51. T. C. W. Mok and A. C. S. Chung, "Learning data augmentation for brain tumor segmentation with coarse-to-fine generative adversarial networks," in *Brainlesion: Glioma, Multiple Sclerosis, Stroke and Traumatic Brain Injuries* (A. Crimi, S. Bakas, H. Kuijff, F. Keyvan, M. Reyes, and T. van Walsum, eds.), (Cham), pp. 70–80, Springer International Publishing, 2019.
52. D. Nie, X. Cao, Y. Gao, L. Wang, and D. Shen, "Estimating CT image from MRI data using 3D fully convolutional networks," in *Deep Learning and Data Labeling for Medical Applications* (G. Carneiro, D. Mateus, L. Peter, A. Bradley, J. M. R. S. Tavares, V. Belagiannis, J. P. Papa, J. C. Nascimento, M. Loog, Z. Lu, J. S. Cardoso, and J. Corneibise, eds.), (Cham), pp. 170–178, Springer International Publishing, 2016.
53. X. Han, "MR-based synthetic CT generation using a deep convolutional neural network method," *Medical Physics*, vol. 44, pp. 1408–1419, Apr. 2017.
54. S. Kida, T. Nakamoto, M. Nakano, K. Nawa, A. Haga, J. Kotoku, H. Yamashita, and K. Nakagawa, "Cone Beam Computed Tomography Image Quality Improvement Using a Deep Convolutional Neural Network," *Cureus*, vol. 10, p. e2548, Apr. 2018.
55. A. Ben-Cohen, E. Klang, S. P. Raskin, S. Soffer, S. Ben-Haim, E. Konen, M. M. Amitai, and H. Greenspan, "Cross-modality synthesis from CT to PET using FCN and GAN networks for improved automated lesion detection," *Engineering Applications of Artificial Intelligence*, vol. 78, pp. 186–194, 2019.
56. J. M. Wolterink, A. M. Dinkla, M. H. F. Savenije, P. R. Seevinck, C. A. T. van den Berg, and I. Išgum, "Deep MR to CT synthesis using unpaired data," in *Simulation and Synthesis in Medical Imaging* (S. A. Tsaftaris, A. Gooya, A. F. Frangi, and J. L. Prince, eds.), (Cham), pp. 14–23, Springer International Publishing, 2017.
57. Y. Hiasa, Y. Otake, M. Takao, T. Matsuoka, K. Takashima, A. Carass, J. Prince, N. Sugano, and Y. Sato, "Cross-modality image synthesis from unpaired data using cycleGAN: Effects of gradient consistency loss and training data size," in *Simulation and Synthesis in Medical Imaging - Third International Workshop, SASHIMI 2018, Held in Conjunction with MICCAI 2018, Proceedings* (O. Goksel, I. Oguz, A. Gooya, and N. Burgos, eds.), Lecture Notes in Computer Science (including subseries Lecture Notes in Artificial Intelligence and Lecture Notes in Bioinformatics), pp. 31–41, Springer Verlag, 1 2018.
58. S. Kida, S. Kaji, K. Nawa, T. Imae, T. Nakamoto, S. Ozaki, T. Ohta, Y. Nozawa, and K. Nakagawa, "Cone-beam CT to planning CT synthesis using generative adversarial networks," 2019. arXiv:1901.05773.
59. Z. Zhang, L. Yang, and Y. Zheng, "Translating and segmenting multimodal medical volumes with cycle- and shape-consistency generative adversarial network," *2018 IEEE/CVF Conference on Computer Vision and Pattern Recognition*, pp. 9242–9251, 2018.
60. E. Wu, K. Wu, D. Cox, and W. Lotter, "Conditional infilling GANs for data augmentation in mammogram classification," in *RAMBO+BIA+TIA@MICCAI*, vol. 11040 of *Lecture Notes in Computer Science*, pp. 98–106, Springer, 2018.
61. J. H. Rick Chang, C.-L. Li, B. Poczos, B. V. K. Vijaya Kumar, and A. C. Sankaranarayanan, "One network to solve them all – solving linear inverse problems using deep projection models," in *The IEEE International Conference on Computer Vision (ICCV)*, Oct 2017.
62. D. Ulyanov, A. Vedaldi, and V. S. Lempitsky, "Deep image prior," in *CVPR*, pp. 9446–9454, IEEE Computer Society, 2018.
63. J. Adler and O. Öktem, "Solving ill-posed inverse problems using iterative deep neural networks," *Inverse Problems*, vol. 33, p. 124007, nov 2017.
64. A. Lucas, M. Iliadis, R. Molina, and A. K. Katsaggelos, "Using deep neural networks for inverse problems in imaging: Beyond analytical methods," *IEEE Signal Processing Magazine*, vol. 35, pp. 20–36, Jan 2018.
65. S. Tokui, K. Oono, S. Hido, and J. Clayton, "Chainer: a next-generation open source framework for deep learning," in *Proceedings of Workshop on Machine Learning Systems (LearningSys) in The Twenty-ninth Annual Conference on Neural Information Processing Systems (NIPS)*, 2015.
66. National Cancer Institute Clinical Proteomic Tumor Analysis Consortium (CPTAC), "Radiology data from the clinical proteomic tumor analysis consortium sarcomas [CPTAC-SAR] collection [data set]." <https://wiki.cancerimagingarchive.net/display/Public/CPTAC-SAR>, 2018.
67. R. Tanno, D. E. Worrall, A. Ghosh, E. Kaden, S. N. Sotiropoulos, A. Criminisi, and D. C. Alexander, "Bayesian image quality transfer with CNNs: Exploring uncertainty in dMRI super-resolution," in *Medical Image Computing and Computer Assisted Intervention - MICCAI 2017 - 20th International Conference, Quebec City, QC, Canada, September 11-13, 2017, Proceedings, Part I*, pp. 611–619, 2017.
68. J. Adler, H. Kohr, and O. Öktem, "Operator discretization library (odl)," Jan. 2017.